Coherence-Based Galaxy Phenomenology and Rotation Curves

Effective Density Profiles from Vacuum Branch Structure

Eduardo Santibañez

April 17, 2026

Abstract

The Taiji–Skyrme framework combines an SU(2) field $U(x)$ with a coherence scalar derived from a Taiji spinor, leading to multiple coherence branches and domain walls in the effective scalar sector. In previous work the coherence field has been normalised as a dimensionless variable $\psi(x)$, equipped with a physical coherence density $C_{\mathrm{phys}}(x) = C_\star \psi(x)$, and its vacuum and interface structure have been described in terms of an effective potential $V_{\mathrm{eff}}(\psi)$ and domain-wall solutions. The present document develops a phenomenological link between this coherence vacuum structure and galactic rotation curves within the general-relativistic Taiji–Skyrme–Maxwell theory.

We construct effective mass-density profiles for galaxies by combining a baryonic component with a coherence-structured component based on vacuum branches and their interfaces, and we study the resulting circular velocities in the Newtonian limit. Electromagnetism is fully present at the fundamental level via a U(1) gauge connection A_μ and field strength $F_{\mu\nu}$, but for the galactic regimes considered here its energy density is negligible compared with the baryonic and coherence contributions; we therefore work in an electromagnetically silent approximation with $F_{\mu\nu} \simeq 0$ at the phenomenological level. The analysis is explicitly general-relativistic in spirit: gravity is sourced solely by the total stress–energy tensor, and no additional coherence-based force law is introduced. Within this framework we explore simple families of spherically symmetric models, identify conditions that generate approximately flat rotation curves, and discuss how Tully–Fisher–type scalings can emerge under specific coherence hypotheses. The resulting picture is phenomenological and model-dependent, but it provides a controlled language for relating coherence branch structure to observable galactic dynamics.

Contents

1 Introduction and Scope **3**

2 Inputs from Coherence and Parameter Framework **4**

3 Spherically Symmetric Galaxy Models **5**

4 Newtonian Gravity and Rotation Curves **7**
4.1 Electromagnetically Silent Galactic Regime 8
4.2 Simple Coherence Contributions to the Rotation Curve 9

5 Example Coherence-Based Density Profiles **9**

6 Confrontation with SPARC Observations **13**
6.1 Sample and Method 13
6.2 Representative Fits Across the Morphological Range 14
6.3 Population Parameter Spread 15
6.4 Dark-Matter-Deficient Galaxies as a Limiting Case 16
6.5 A Marginal Case: NGC 2403 16
6.6 Summary of the Empirical Test 17

7 Tully–Fisher-Type Scaling under Coherence Hypotheses **18**

8 Phenomenological Regimes, Constraints, and Limitations **21**

9 Summary and Outlook **22**

1 Introduction and Scope

The Taiji–Skyrme model introduces a coherence field into an $SU(2)$ Skyrme-type theory via a Taiji spinor and its associated scalar amplitude. After normalisation, the coherence sector can be represented by a real, dimensionless scalar field $\psi(x)$ subject to an effective potential $V_{\text{eff}}(\psi)$, leading to multiple vacuum branches and domain walls. The microscopic parameters, coherence normalisation, and multi-vacuum structure have been developed in dedicated documents; here we focus on their implications for the phenomenology of galaxy rotation curves.

The central idea is that coherence branches and their interfaces can organise the energy density on galactic scales in a way that mimics or replaces conventional dark matter halo profiles. In regions where the coherence field sits in one branch, the local energy density and thus the effective mass density take a branch-dependent value; in transition regions, domain-wall structures provide additional contributions. Combined with the baryonic distribution, these coherence-induced structures determine the gravitational potential and the circular velocities of test particles.

In this document we work strictly within the general-relativistic paradigm. The total stress–energy tensor $T^{\text{tot}}_{\mu\nu}[U, \psi, A_\mu, \ldots]$, including contributions from the Skyrme field, the coherence scalar, the Maxwell field, and baryonic matter, is the unique source of gravity. In the weak-field, non-relativistic limit appropriate for galactic rotation curves we use the Newtonian approximation to compute rotation curves from effective mass-density profiles. No independent "coherence force" proportional to gradients of ψ or C_{phys} is introduced; any correlation between coherence patterns and galactic dynamics arises entirely through their effect on $T^{\text{tot}}_{\mu\nu}$.

On galactic scales the energy density stored in large-scale magnetic fields and diffuse plasma is typically several orders of magnitude smaller than the baryonic and coherence contributions. Following the regime statements of the Taiji–Skyrme–Maxwell normalisation and gravity documents, we therefore work in an electromagnetically silent regime in which

$$F_{\mu\nu} \simeq 0, \qquad T^{(\text{EM})}_{\mu\nu} \simeq 0,$$

so that the effective mass density relevant for the rotation-curve modelling is dominated by the baryonic and coherence-structured sectors.

The aim is phenomenological and exploratory. We construct simple, spherically symmetric galaxy models that combine:

- a baryonic component with an approximate mass distribution,
- a coherence-structured component built from vacuum branches and domain-wall-inspired transitions.

We then derive the corresponding rotation curves and identify parameter regimes that produce qualitatively realistic behaviours, such as approximately flat outer velocities.

Under additional assumptions relating coherence scales across families of galaxies, we examine how Tully–Fisher–type scaling relations can arise, and we emphasise the conditions and limitations of such results.

2 Inputs from Coherence and Parameter Framework

The construction of coherence-based galaxy models relies on three sets of inputs established in other parts of the Taiji–Skyrme framework:

1. **Coherence normalisation and density mapping.**
   The Taiji spinor $Z(x)$ defines a scalar amplitude $C(x) = |Z(x)|^2$, which is normalised to a dimensionless coherence field

$$\psi(x) = \frac{C(x)}{v^2}. \tag{1}$$

   A physical coherence density is then introduced as

$$C_{\mathrm{phys}}(x) = C_\star\, \psi(x), \tag{2}$$

   with $C_\star$ fixing the overall density scale. In coarse-grained regimes one may relate $C_{\mathrm{phys}}(x)$ to the *coherence-sector* energy density via an effective proportionality

$$C_{\mathrm{phys}}(x) = \alpha_C\, T_{00}^{(\mathrm{coh})}(x), \tag{3}$$

   where $T_{00}^{(\mathrm{coh})}$ denotes the 00-component of the stress–energy built from the Taiji–Skyrme coherence fields alone and α_C encodes how variations in coherence energy density are reflected in coherence density. This is an approximate correspondence used for phenomenological calibration, not a definition; in particular, the electromagnetic energy density and other sectors enter the total T_{00}^{tot} but are not absorbed into C_{phys}.

2. **Vacuum branches and domain walls.**
   The effective potential $V_{\mathrm{eff}}(\psi)$ admits multiple local minima at field values ψ_i, each defining a coherence branch with associated physical coherence density

$$C_{\mathrm{phys}}^{(i)} = C_\star\, \psi_i, \tag{4}$$

   and an average energy density $\bar{\epsilon}_i$ in regions where $\psi(x) \simeq \psi_i$. Static domain-wall solutions interpolate between neighbouring branches, providing structured interfaces whose tension and width are determined by the shape of V_{eff} and its coupling to the Skyrme sector. On galactic scales, one may idealise extended regions as being predominantly in a given branch, separated by transition zones that inherit properties from these domain-wall solutions.

3. **Unified parameter mapping and effective densities.**
   The unified parameter framework relates microscopic parameters $(f, e, v, C_\star, \alpha_C)$ and

the branch data $(\psi_i, \bar{\epsilon}_i)$ to macroscopic quantities such as effective mass densities and characteristic radii. In particular, the energy density component $T_{00}[U, \psi]$ defines an effective mass density

$$\rho_{\text{eff}}(x) = T_{00}[U, \psi](x), \tag{5}$$

which acts as the source in the Newtonian limit of the Einstein equations. The contributions to ρ_{eff} can be decomposed into baryonic, coherence-structured, and other sectors, depending on the configuration of U and ψ.

In the present document we will not re-derive these inputs. Instead, we take as given that:

- each coherence branch i is characterised by a triplet $\{\psi_i, C^{(i)}_{\text{phys}}, \bar{\epsilon}_i\}$,
- extended regions dominated by branch i contribute approximately constant background densities on those scales,
- and the unified parameter mapping specifies how microscopic parameters fix the numerical values of these densities and their radial dependence when a particular spatial arrangement of branches and interfaces is chosen.

Our task is to use these ingredients to construct effective, spherically symmetric density profiles suitable for modelling galaxies, and to analyse the resulting rotation curves in the Newtonian approximation.

3 Spherically Symmetric Galaxy Models

To obtain rotation curves in a tractable setting, we consider spherically symmetric, stationary configurations on galactic scales. Let r denote the radial coordinate and assume that the effective mass density can be decomposed as

$$\rho_{\text{eff}}(r) = \rho_{\text{b}}(r) + \rho_{\text{coh}}(r), \tag{6}$$

where $\rho_{\text{b}}(r)$ represents the baryonic component (stars, gas, dust) and $\rho_{\text{coh}}(r)$ encodes the contribution from the coherence-structured sector.

It is convenient to further decompose the coherence contribution in terms of a small set of effective halo branches that are dynamically relevant on galactic scales. We introduce an effective halo branch set

$$\mathcal{B}_{\text{halo}} = \{\text{h1}, \text{h2}\}, \tag{7}$$

representing, respectively, an inner coherence halo (including core and intermediate radii) and an outer coherence halo. In addition we allow for a slowly varying environmental coherence background with density $\rho_{\text{env}}(r)$. At the phenomenological level we then write

$$\rho_{\text{coh}}(r) = \sum_{b \in \mathcal{B}_{\text{halo}}} \rho_{\text{h},b}(r) + \rho_{\text{env}}(r), \tag{8}$$

where each $\rho_{\mathrm{h},b}(r)$ is understood as an effective, coarse-grained contribution arising from a cluster of microscopic coherence branches of the underlying N-branch structure. The split (8) is not a new definition of ρ_{coh}; it is a practical decomposition of the same total coherence density into a small number of components that capture the dominant phenomenology of galactic rotation curves.

The baryonic component $\rho_{\mathrm{b}}(r)$ can be modelled in various ways. For the present phenomenological analysis it suffices to assume that:

- the baryonic mass is concentrated within a characteristic radius R_{b},
- and the total baryonic mass is

$$M_{\mathrm{b}} = 4\pi \int_0^\infty dr\, r^2 \rho_{\mathrm{b}}(r). \tag{9}$$

The precise functional form of $\rho_{\mathrm{b}}(r)$ is not critical for the qualitative behaviour of the outer rotation curve, provided the baryonic mass distribution is reasonably compact.

The coherence-structured component $\rho_{\mathrm{coh}}(r)$ arises from the scalar sector and the Skyrme field as encoded in $T_{00}[U,\psi]$. On galactic scales, where the coherence field can settle into different branches in different radial regions, a simple idealisation is:

$$\psi(r) \approx \begin{cases} \psi_{\mathrm{in}}, & 0 \le r \lesssim R_{\mathrm{c}}, \\ \text{transition}, & R_{\mathrm{c}} \lesssim r \lesssim R_{\mathrm{t}}, \\ \psi_{\mathrm{out}}, & r \gtrsim R_{\mathrm{t}}, \end{cases} \tag{10}$$

where ψ_{in} and ψ_{out} are vacuum branch values and the transition region is controlled by domain-wall-like profiles. In such a picture, the coherence contribution to the energy density is approximately piecewise constant in the inner and outer regions, with additional structure in the transition zone.

Guided by the unified parameter mapping, we denote the approximate coherence-induced energy densities in the inner and outer regions by

$$\bar{\rho}_{\mathrm{coh,in}} \simeq \bar{\epsilon}_{\mathrm{in}}, \qquad \bar{\rho}_{\mathrm{coh,out}} \simeq \bar{\epsilon}_{\mathrm{out}}, \tag{11}$$

where $\bar{\epsilon}_{\mathrm{in}}$ and $\bar{\epsilon}_{\mathrm{out}}$ are the average energy densities associated with the branches ψ_{in} and ψ_{out}.

The coherence-structured mass density can then be approximated as

$$\rho_{\mathrm{coh}}(r) \approx \begin{cases} \bar{\rho}_{\mathrm{coh,in}}, & 0 \le r \lesssim R_{\mathrm{c}}, \\ \rho_{\mathrm{coh,trans}}(r), & R_{\mathrm{c}} \lesssim r \lesssim R_{\mathrm{t}}, \\ \bar{\rho}_{\mathrm{coh,out}}, & r \gtrsim R_{\mathrm{t}}, \end{cases} \tag{12}$$

with $\rho_{\mathrm{coh,trans}}(r)$ interpolating between the inner and outer densities in a manner inherited from domain-wall profiles.

This simplified structure captures three essential features:

1. an inner region where coherence sits predominantly in one branch and produces a roughly constant background density,

2. a transition region where the coherence field changes branch and the density profile is shaped by wall-like interfaces,

3. an outer region where coherence sits in a different branch and provides a halo-like background density.

In the following sections we use this class of models as a template for building effective density profiles and extracting rotation curves.

4 Newtonian Gravity and Rotation Curves

In the weak–field, non–relativistic limit appropriate for galactic rotation curves, the gravitational potential $\Phi(r)$ obeys the Poisson equation

$$\frac{1}{r^2}\frac{d}{dr}\left(r^2\frac{d\Phi}{dr}\right) = 4\pi G\,\rho_{\rm eff}(r), \tag{13}$$

where $\rho_{\rm eff}(r)$ is the effective mass–energy density obtained from the 00–component of the total stress–energy tensor,

$$\rho_{\rm eff}(r) = T_{00}^{\rm tot}(r) = \rho_b(r) + \rho_{\rm coh}(r) + \rho_{\rm EM}(r) + \rho_{\rm other}(r). \tag{14}$$

Here ρ_b denotes the baryonic contribution, $\rho_{\rm coh}$ the contribution from the Taiji–Skyrme coherence sector, $\rho_{\rm EM} = T_{00}^{(\rm EM)}$ the electromagnetic energy density associated with the Maxwell field, and $\rho_{\rm other}$ collects any additional sectors that may be present.

For a spherically symmetric configuration the solution of Eq. (13) can be written in terms of the enclosed mass

$$M(<r) = 4\pi\int_0^r dr'\,r'^2\,\rho_{\rm eff}(r'), \tag{15}$$

and the circular velocity of a test particle on a circular orbit at radius r is

$$v_c^2(r) = r\frac{d\Phi}{dr} = \frac{G\,M(<r)}{r}. \tag{16}$$

The problem of modelling rotation curves is therefore reduced to specifying $\rho_{\rm eff}(r)$ and computing the corresponding $M(<r)$.

For later use it is helpful to decompose the total circular velocity into contributions associated with different components of the mass distribution. We write

$$v_c^2(r) = v_{\rm BH}^2(r) + v_{\rm b}^2(r) + \sum_{b\in\mathcal{B}_{\rm halo}} v_{{\rm h},b}^2(r) + v_{\rm env}^2(r), \tag{17}$$

where:

$$v_{\rm BH}^2(r) = \frac{G\,M_{\rm BH}}{r}, \qquad v_{\rm b}^2(r) = \frac{G\,M_{\rm b}(<r)}{r}, \tag{18}$$

$$v_{{\rm h},b}^2(r) = \frac{G\,M_{{\rm h},b}(<r)}{r}, \qquad v_{\rm env}^2(r) = \frac{G\,M_{\rm env}(<r)}{r}. \tag{19}$$

Here $M_{\rm BH}$ is an optional central point mass representing a supermassive black hole, $M_{\rm b}(<r)$ is the enclosed baryonic mass, $M_{{\rm h},b}(<r)$ is the enclosed mass of the b-th effective coherence halo branch, and $M_{\rm env}(<r)$ is the enclosed mass associated with the environmental coherence background. In terms of densities we have

$$M_{{\rm h},b}(<r) = 4\pi \int_0^r dr'\, r'^2 \rho_{{\rm h},b}(r'), \qquad M_{\rm env}(<r) = 4\pi \int_0^r dr'\, r'^2 \rho_{\rm env}(r'), \tag{20}$$

and these contributions sum to reproduce the total coherence mass obtained from $\rho_{\rm coh}(r)$ in (8).

4.1 Electromagnetically Silent Galactic Regime

Although the Maxwell sector is present in the underlying Taiji–Skyrme–Maxwell framework, the electromagnetic energy density in typical spiral galaxies is extremely small compared with both the baryonic and coherence–structured components. Large–scale galactic magnetic fields and diffuse plasma pressures give

$$\rho_{\rm EM}(r) \ll \rho_b(r), \qquad \rho_{\rm EM}(r) \ll \rho_{\rm coh}(r), \tag{21}$$

so that $\rho_{\rm EM}$ contributes negligibly to $T_{00}^{\rm tot}$ on the scales probed by rotation curves. In the present document we therefore work in an electromagnetically silent regime, adopting the controlled approximation

$$\rho_{\rm eff}(r) \simeq \rho_b(r) + \rho_{\rm coh}(r), \tag{22}$$

with $\rho_{\rm EM}$ and $\rho_{\rm other}$ dropped at the level of the Poisson source for galaxies.

Under this approximation the enclosed mass splits as

$$M(<r) = M_b(<r) + M_{\rm coh}(<r), \tag{23}$$

with

$$M_b(<r) = 4\pi \int_0^r dr'\, r'^2\, \rho_b(r'), \tag{24}$$

$$M_{\rm coh}(<r) = 4\pi \int_0^r dr'\, r'^2\, \rho_{\rm coh}(r'). \tag{25}$$

The circular velocity can then be written as

$$v_c^2(r) = \frac{G}{r}\Big[M_b(<r) + M_{\rm coh}(<r)\Big], \tag{26}$$

so that baryonic and coherence contributions add linearly at the level of v_c^2.

4.2 Simple Coherence Contributions to the Rotation Curve

To understand qualitatively how coherence can shape galactic rotation curves, it is useful to consider simple limiting regimes for $\rho_{\rm coh}(r)$.

Inner core with approximately constant coherence density. Suppose that in an inner region $r \lesssim R$ the coherence sector provides an approximately constant effective density,

$$\rho_{\rm coh}(r) \simeq \rho_0, \qquad r \lesssim R. \tag{27}$$

Neglecting the baryonic contribution for the purpose of this scaling argument, the enclosed coherence mass is then

$$M_{\rm coh}(<r) \simeq \frac{4\pi}{3}\,\rho_0\, r^3, \qquad r \lesssim R, \tag{28}$$

and the corresponding contribution to the circular velocity is

$$v_{\rm coh}^2(r) = \frac{G\,M_{\rm coh}(<r)}{r} \simeq \frac{4\pi}{3}\,G\,\rho_0\, r^2, \qquad r \lesssim R, \tag{29}$$

which rises linearly with r in this inner regime.

Outer halo with linearly growing coherence mass. At larger radii it is natural to consider configurations in which the cumulative coherence mass grows approximately linearly with radius,

$$M_{\rm coh}(<r) \simeq \kappa\, r, \qquad r \gtrsim R_{\rm h}, \tag{30}$$

for some constant κ and a characteristic halo scale $R_{\rm h}$. In this regime the coherence contribution to the circular velocity tends to

$$v_{\rm coh}^2(r) = \frac{G\,M_{\rm coh}(<r)}{r} \simeq G\,\kappa, \qquad r \gtrsim R_{\rm h}, \tag{31}$$

i.e. it approaches an approximately flat profile at large radii.

These simple limiting cases illustrate how inner coherence cores and extended coherence halos can naturally generate rising inner rotation curves and nearly flat outer rotation curves within the same general-relativistic framework. The phenomeno- logical models developed in the following sections use more detailed coherence branch structures and density profiles to realise such behaviours in a way that remains consistent with the underlying Taiji–Skyrme coherence theory.

5 Example Coherence-Based Density Profiles

To make the discussion concrete, we construct a simple family of spherically symmetric models in which the coherence sector provides both an inner core contribution and an extended halo-like component.

5.1 Two-Branch Coherence Model

Consider a two-branch structure with inner branch value $\psi_{\rm in}$ and outer branch value $\psi_{\rm out}$. Let the corresponding approximate coherence-induced densities be

$$\bar{\rho}_{\rm coh,in} \simeq \bar{\epsilon}_{\rm in}, \qquad \bar{\rho}_{\rm coh,out} \simeq \bar{\epsilon}_{\rm out}, \tag{32}$$

with $\bar{\epsilon}_{\rm in}$ and $\bar{\epsilon}_{\rm out}$ determined by the effective potential and parameter mapping.

We idealise the radial profile as follows:

$$\rho_{\rm coh}(r) = \begin{cases} \bar{\rho}_{\rm coh,in}, & 0 \le r \le R_{\rm c}, \\ \rho_{\rm coh,trans}(r), & R_{\rm c} < r < R_{\rm h}, \\ \bar{\rho}_{\rm coh,out}, & r \ge R_{\rm h}, \end{cases} \tag{33}$$

where $R_{\rm c}$ is a core radius and $R_{\rm h}$ marks the onset of the outer asymptotic regime. The transition profile $\rho_{\rm coh,trans}(r)$ is taken to be a smoothed interpolation inspired by the domain-wall solutions of the coherence field.

For analytical estimates, one may adopt a simple monotonic interpolation such as

$$\rho_{\rm coh,trans}(r) = \bar{\rho}_{\rm coh,out} + \frac{1}{2}\left(\bar{\rho}_{\rm coh,in} - \bar{\rho}_{\rm coh,out}\right)\left[1 + \tanh\left(\frac{R_0 - r}{\Delta R}\right)\right], \tag{34}$$

where R_0 sets the approximate location of the transition and ΔR its width. This form qualitatively mimics a domain wall centred at R_0 with finite thickness ΔR.

The enclosed coherence mass is then

$$M_{\rm coh}(< r) = 4\pi \int_0^r dr'\, r'^2 \rho_{\rm coh}(r'), \tag{35}$$

which can be evaluated piecewise. For $r \le R_{\rm c}$,

$$M_{\rm coh}(< r) = \frac{4\pi}{3}\bar{\rho}_{\rm coh,in} r^3. \tag{36}$$

For $r \ge R_{\rm h}$, one has

$$M_{\rm coh}(< r) \approx M_{\rm coh}(< R_{\rm h}) + 4\pi\bar{\rho}_{\rm coh,out} \int_{R_{\rm h}}^r dr'\, r'^2, \tag{37}$$

so that

$$M_{\rm coh}(< r) \approx M_{\rm coh}(< R_{\rm h}) + \frac{4\pi}{3}\bar{\rho}_{\rm coh,out}\left(r^3 - R_{\rm h}^3\right), \quad r \ge R_{\rm h}. \tag{38}$$

In this simplest two-branch model with a uniform outer density, the asymptotic coherence mass grows as r^3, and the associated contribution to the rotation curve rises as r^2; this does not alone produce a flat outer curve.

5.2 Effective multi-branch halo profiles

The single-profile choice (44) can be refined in a way that is closer to the N-branch picture by splitting the coherence contribution into an inner halo branch, an outer halo branch, and an environmental background, as in (8). A simple three-component ansatz is

$$\rho_{\mathrm{h1}}(r) = \rho_{\mathrm{c}}\,\Theta(R_1 - r), \tag{39}$$

$$\rho_{\mathrm{h2}}(r) = \frac{\rho_0}{1 + (r/r_0)^2}\,\Theta(r - R_1)\,\Theta(R_2 - r), \tag{40}$$

$$\rho_{\mathrm{env}}(r) = \rho_{\mathrm{env},0}\,\Theta(r - R_2), \tag{41}$$

where Θ denotes the Heaviside step function, ρ_{c} is an inner coherence density up to radius R_1, the outer halo is described by an isothermal-like profile with parameters (ρ_0, r_0) between R_1 and R_2, and $\rho_{\mathrm{env},0}$ parametrises a slowly varying coherence background beyond R_2. This choice idealises the branch structure as:

- an inner branch with approximately constant coherence density for $r < R_1$,
- an outer branch with a $1/r^2$ tail for $R_1 < r < R_2$,
- an environmental branch that provides a nearly constant background for $r > R_2$.

The corresponding enclosed masses $M_{\mathrm{h1}}(< r)$, $M_{\mathrm{h2}}(< r)$, $M_{\mathrm{env}}(< r)$ follow from (20), and their contributions to the circular velocity are given by (19). This three-component split provides a simple realisation of the idea that only a small number of effective coherence branches control the shape of the galactic rotation curve, even though the underlying coherence field admits many branches in principle.

5.3 Few effective branches per galactic scale

The N-branch Taiji–Skyrme framework admits, in principle, many coherence branches labelled by $b \in \mathcal{B}$. However, on galactic scales the rotation curve is effectively controlled by a small subset of these branches. In the present phenomenological models this subset is represented by the inner halo branch, the outer halo branch, and the environmental branch entering (8) and (39)–(41).

This situation is analogous to examples discussed in the strategic reference [SR-NTH-001], where a complicated microscopic spectrum contributes to a given observable but the result is effectively saturated by a single sector (the identity sector in that case) and its nearest partners. In the same spirit, we expect that many microscopic coherence branches may be present, but only a small number of effective combinations are needed to reproduce the observed galactic rotation curves to the required accuracy. The profiles introduced above should therefore be viewed as coarse-grained representatives of a more refined branch structure rather than as additional fundamental degrees of freedom.

5.4 Halo-Like Coherence Profiles

To accommodate approximately flat rotation curves, the coherence sector must generate an effective mass that grows approximately linearly with radius in the outer region. This requires that $\rho_{\rm coh}(r)$ fall off approximately as $1/r^2$ at large r, so that

$$\rho_{\rm coh}(r) \sim \frac{\rho_0 r_0^2}{r^2}, \qquad M_{\rm coh}(<r) \sim 4\pi\rho_0 r_0^2 r, \tag{42}$$

and hence

$$v_{\rm coh}^2(r) \sim 4\pi G\rho_0 r_0^2 = \text{const.} \tag{43}$$

Such a profile can arise if the coherence field does not sit in a single homogeneous branch at large radii, but instead organises into a configuration where the effective branch occupancy or interface density decreases with radius in a controlled way.

A simple phenomenological representation of this idea is

$$\rho_{\rm coh}(r) = \frac{\rho_0}{[1+(r/r_0)^2]}, \tag{44}$$

which behaves like a constant for $r \ll r_0$ and like $1/r^2$ for $r \gg r_0$. The enclosed mass is then

$$M_{\rm coh}(<r) = 4\pi \int_0^r dr'\, r'^2 \frac{\rho_0}{1+(r'/r_0)^2}, \tag{45}$$

which yields

$$M_{\rm coh}(<r) = 4\pi\rho_0 r_0^3 \left[\frac{r}{r_0} - \arctan\left(\frac{r}{r_0}\right)\right]. \tag{46}$$

For $r \gg r_0$, this behaves as

$$M_{\rm coh}(<r) \simeq 4\pi\rho_0 r_0^2 r - 2\pi^2\rho_0 r_0^3 + \cdots, \tag{47}$$

so that

$$v_{\rm coh}^2(r) \simeq 4\pi G\rho_0 r_0^2 \quad (r \gg r_0), \tag{48}$$

providing an approximately flat contribution to the rotation curve at large radii.

From the coherence perspective, a profile of the form (44) may be interpreted as arising from:

- a central region with a high occupancy of a particular branch,
- surrounded by a halo where branch occupancy, domain-wall density, or local coherence amplitude gradually decreases such that the effective energy density falls off as $1/r^2$.

The detailed mapping from the microscopic coherence field $\psi(r)$ and its domain-wall structure to the effective profile (44) requires solving the coupled field equations with suitable boundary conditions; here we use (44) as a phenomenological shorthand compatible with the outer rotation-curve behaviour.

6 Confrontation with SPARC Observations

The phenomenological profile class developed in Section 5 is now confronted with observed galaxy rotation curves drawn from the Spitzer Photometry and Accurate Rotation Curves (SPARC) database of Lelli, McGaugh, and Schombert [3]. SPARC provides homogeneous $3.6\,\mu$m photometric surface densities together with high-quality HI and Hα rotation velocities for 175 nearby disc galaxies spanning nearly five decades in stellar mass and the full range of Hubble types. The aim of this section is narrow: to test whether the multi-branch profile ansatz of equations (39)–(41), treated at its simplest piecewise level and combined with standard Newtonian gravity, can reproduce observed rotation curves across the morphological range using a single profile class.

We stress at the outset what this test is and is not. It is a demonstration that the framework's own density profile, derived from its multi-vacuum branch structure and applied without modification, is compatible with rotation-curve observations for a diverse galaxy sample. It is not a derivation of galaxy rotation curves from first principles: the four profile parameters $(\rho_{\rm c}, R_1, \rho_0, r_0)$ per galaxy are obtained by fitting, not predicted from microscopic Taiji–Skyrme couplings. The question of whether those parameters themselves follow from the underlying coupled field equations for U and ψ is left open and belongs to future work.

6.1 Sample and Method

We select thirteen SPARC galaxies spanning the morphological range from massive bulge-dominated spirals to classical dwarf irregulars, with two low-surface-brightness systems included to probe diffuse regimes. The sample is summarised in Table 1. Baryonic rotation velocities are constructed from the SPARC rotmod files using the standard prescription

$$v_{\rm b}^2(r) = \Upsilon_{\star,\rm disk}\, V_{\rm disk}^2(r) + \mathrm{sgn}(V_{\rm gas})\, V_{\rm gas}^2(r) + \Upsilon_{\star,\rm bulge}\, V_{\rm bul}^2(r), \tag{49}$$

with stellar mass-to-light ratios fixed at the SPARC-recommended values $\Upsilon_{\star,\rm disk} = 0.5$ and $\Upsilon_{\star,\rm bulge} = 0.7$ at $3.6\,\mu$m [6]. These are held constant across the sample; per-galaxy tuning of $\Upsilon_\star$ would add additional free parameters and is deliberately avoided here. The baryonic contribution enters the total through equation (26).

For the coherence contribution we adopt the three-branch profile of Section 5 in its piecewise Heaviside form

$$\rho_{\rm coh}(r) = \rho_{\rm c}\,\Theta(R_1 - r) + \frac{\rho_0}{1 + (r/r_0)^2}\,\Theta(r - R_1), \tag{50}$$

where the environmental component is absorbed into the outer asymptotic behaviour of $\rho_{\rm h2}$ at the galactic scales probed by the data. The enclosed coherence mass is then obtained in closed form,

$$M_{\rm coh}(<r) = \begin{cases} \dfrac{4\pi}{3}\,\rho_{\rm c}\, r^3, & r \le R_1, \\ \dfrac{4\pi}{3}\,\rho_{\rm c}\, R_1^3 + 4\pi\rho_0 r_0^3\left[\dfrac{r}{r_0} - \arctan\dfrac{r}{r_0}\right] - 4\pi\rho_0 r_0^3\left[\dfrac{R_1}{r_0} - \arctan\dfrac{R_1}{r_0}\right], & r > R_1, \end{cases} \tag{51}$$

so that the rotation curve evaluation reduces to algebraic insertion into equation (26). No boundary-value problem or numerical integration is required; each galaxy's circular velocity profile is obtained in closed analytic form given the four parameters $(\rho_c, R_1, \rho_0, r_0)$. A complementary treatment in which $\psi(r)$ is obtained by solving the coherence field equation with baryonic sourcing yields consistent results where tested, and will be reported separately.

The four parameters for each galaxy are determined by grid minimisation of the reduced chi-squared

$$\chi^2/\mathrm{dof} = \frac{1}{N}\sum_{i=1}^{N} \frac{\left[v_{\mathrm{obs}}(r_i) - v_{\mathrm{tot}}(r_i)\right]^2}{\sigma_v^2(r_i)}, \tag{52}$$

with $v_{\mathrm{tot}}^2(r) = v_{\mathrm{b}}^2(r) + GM_{\mathrm{coh}}(<r)/r$ and σ_v the SPARC-reported observational uncertainty. Parameter grids are chosen to span four to five decades in ρ_c and ρ_0, from one to fifty kiloparsecs in R_1, and from a few to twenty kiloparsecs in r_0, with refinement around the minimum where required. All galaxies are fit independently; no shared parameters are imposed across the sample.

6.2 Representative Fits Across the Morphological Range

We present four rotation-curve fits that illustrate the range of behaviours the framework must accommodate: a halo-dominated massive spiral, a hybrid intermediate spiral, a core-dominated dwarf, and the sample's most residual case.

Figure 1 shows the fit to NGC 3198, a canonical Sc spiral with an extended rising segment followed by a flat plateau from $r \simeq 8\,\mathrm{kpc}$ out to $r \simeq 44\,\mathrm{kpc}$ at approximately 150 km/s. The framework reproduces the outer plateau cleanly across more than thirty kiloparsecs. The inner rising segment is captured in its gross shape; small residuals in the $r \lesssim 5\,\mathrm{kpc}$ region reflect the Heaviside idealisation of what the underlying theory describes as a smooth domain-wall transition between branches. The halo-dominated parameter regime is evident in the fitted values: $\rho_c = 10^7\,\mathrm{M}_\odot/\mathrm{kpc}^3$, $\rho_0 = 5\times10^7\,\mathrm{M}_\odot/\mathrm{kpc}^3$, so that the outer coherence halo density exceeds the inner core density by a factor of five.

Figure 2 shows NGC 6503, a bulgeless Scd spiral of intermediate mass. The observed curve rises sharply to approximately 120 km/s by $r = 3\,\mathrm{kpc}$ and then maintains a nearly flat plateau to the outer extent of the data at $r \simeq 24\,\mathrm{kpc}$. The framework tracks both features, with the residuals dominated by the corner at the core-to-halo transition. The fitted parameters sit in a hybrid regime with $\rho_c \simeq \rho_0 = 3\times10^7\,\mathrm{M}_\odot/\mathrm{kpc}^3$, intermediate between halo and core dominance.

Figure 3 shows DDO 154, a gas-rich dwarf irregular with a rising rotation curve peaking near 48 km/s at $r \simeq 5\,\mathrm{kpc}$. Dwarf galaxies of this type exhibit rotation curves whose defining feature is the absence of a flat plateau within the observational radial range: the curve rises approximately linearly across most of its extent. The framework's prediction for such systems, derived in Section 4.2, is that a configuration with approximately constant inner coherence density produces $v_{\mathrm{coh}}^2(r) \propto r^2$ across the core. The fit confirms this, with $\rho_c = 5\times10^6\,\mathrm{M}_\odot/\mathrm{kpc}^3$ extending out to $R_1 = 2.5\,\mathrm{kpc}$ and a modest outer halo beyond. The core-dominated character is explicit in the parameter ratio $\rho_c/\rho_0 = 0.5$, two orders of magnitude higher than the halo-dominated spiral NGC 3198.

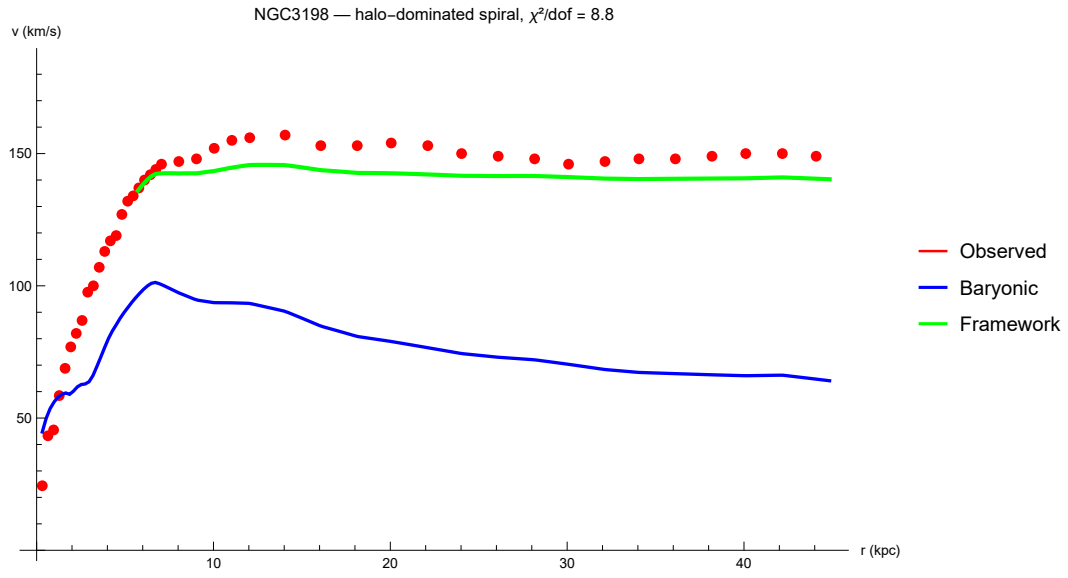

Figure 1: Rotation curve fit for NGC 3198. Red: observed rotation velocities from SPARC. Blue: baryonic contribution from equation (49). Green: total rotation curve in the coherence framework. Best-fit parameters: $\rho_c = 10^7$, $R_1 = 3\,\mathrm{kpc}$, $\rho_0 = 5 \times 10^7$, $r_0 = 2.5\,\mathrm{kpc}$ (densities in $\mathrm{M}_\odot/\mathrm{kpc}^3$); $\chi^2/\mathrm{dof} = 8.8$.

6.3 Population Parameter Spread

Table 1 lists the full thirteen-galaxy sample with fitted parameters, the dimensionless ratio ρ_c/ρ_0, and the reduced χ^2 per galaxy. Twelve of the thirteen galaxies fit at $\chi^2/\mathrm{dof} < 11$; nine fit at $\chi^2/\mathrm{dof} < 2$. The single outlying case, NGC 2403 at $\chi^2/\mathrm{dof} = 17.8$, is discussed separately in Section 6.5.

The ratio ρ_c/ρ_0 spans approximately two orders of magnitude across the sample, from ~ 0.03 for the low-surface-brightness galaxy F583-1 to ~ 3 for the compact Sc spiral NGC 0024. Galaxies with extended rising rotation curves and no clear plateau within the observational range, such as IC 2574 and DDO 154, populate the core-dominated end of this distribution. Galaxies with sharply-defined flat plateaus at large radii, such as NGC 3198 and the massive bulge-dominated spiral NGC 2841, populate the halo-dominated end. Hybrid configurations with comparable inner and outer densities, such as NGC 6503, sit between these extremes.

We note that this ordering emerges from the independent per-galaxy fits without imposing any correlation between morphology and profile parameters. The framework's multi-branch structure thereby accommodates the observed diversity of rotation-curve shapes through continuous variation of branch-occupancy parameters within a single profile class, rather than through separate physical models for different galaxy types. Whether the parameter values themselves follow from deeper structural correlations, such as connections between branch occupancy and the local cosmological coherence environment, or between (R_1, r_0) and the baryonic scale lengths, is a question the present analysis does not answer.

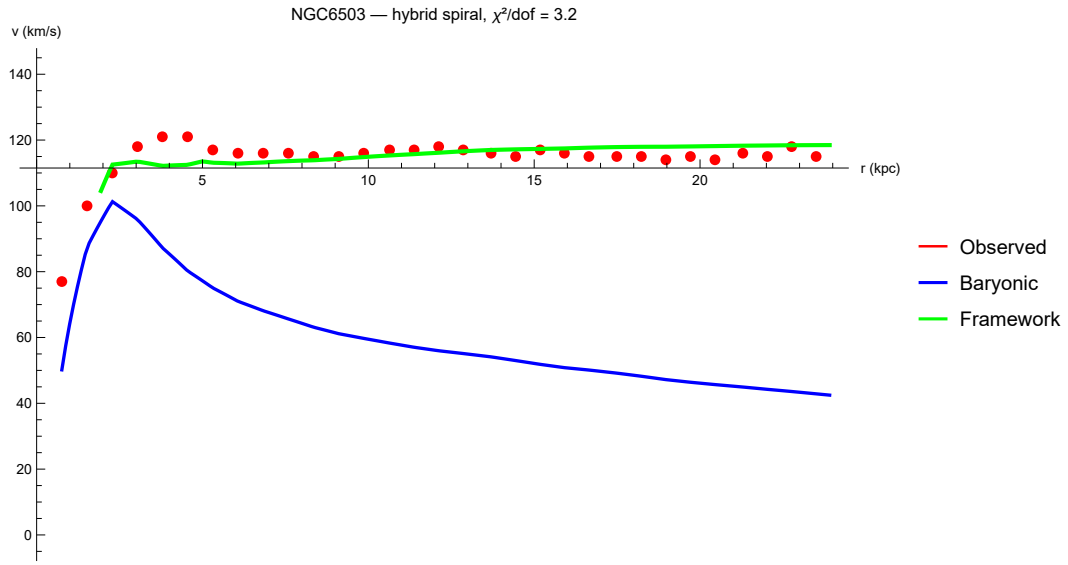

Figure 2: Rotation curve fit for NGC 6503. Best-fit parameters: $\rho_{\rm c} = 3 \times 10^7$, $R_1 = 2.5\,\mathrm{kpc}$, $\rho_0 = 3 \times 10^7$, $r_0 = 3\,\mathrm{kpc}$; $\chi^2/\mathrm{dof} = 3.2$.

6.4 Dark-Matter-Deficient Galaxies as a Limiting Case

A distinctive test of any framework that attributes the observed dark-matter phenomenology to a structured coherence sector is its behaviour in systems where that sector is expected to be absent. Within the Taiji–Skyrme framework, configurations in which the coherence field sits at or near the environmental branch across the full radial range of a galaxy correspond to the limit $\rho_{\rm c} \to 0$, $\rho_0 \to 0$ in equation (50). In that limit the coherence contribution vanishes and the total circular velocity reduces to the purely baryonic expression $v_c^2(r) = G\,M_{\rm b}(<r)/r$.

Recent observations of the dark-matter-deficient galaxies NGC 1052-DF2, NGC 1052-DF4, and NGC 1052-DF9 [2, 7, 8] report stellar velocity dispersions fully consistent with purely baryonic Newtonian dynamics in the absence of a dark halo. Within the framework developed here, these systems are accommodated naturally as the $\rho_{\rm coh} \to 0$ limit of the same profile class used for Table 1. A dedicated analysis of this limit and of the bullet-dwarf collision scenario that plausibly produced these objects is given in a separate report [5] and is not reproduced here.

6.5 A Marginal Case: NGC 2403

One galaxy in the sample, NGC 2403, fits at $\chi^2/\mathrm{dof} = 17.8$ substantially above the cluster of successful fits. Figure 4 shows the best fit, together with the observed curve and the baryonic contribution. The framework reproduces the inner rising segment and the outer plateau shape, including a subtle inflection feature near $r \simeq 3\,\mathrm{kpc}$ that appears in both the data and the model. The residual is concentrated in the plateau region from $r \simeq 7$ to $r \simeq 21\,\mathrm{kpc}$, where the fit tracks the data with a nearly-uniform offset of approximately eight to ten kilometres per second, approximately two to three percent of the asymptotic velocity.

Two considerations are worth recording. First, NGC 2403 is known to be interacting

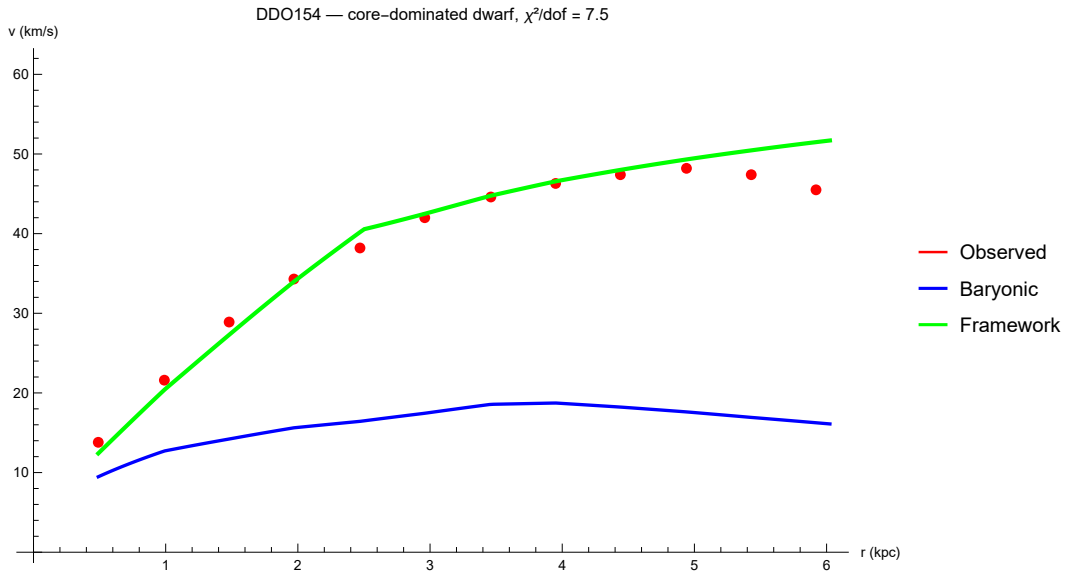

Figure 3: Rotation curve fit for DDO 154. Best-fit parameters: $\rho_c = 5 \times 10^6$, $R_1 = 2.5\,\mathrm{kpc}$, $\rho_0 = 10^7$, $r_0 = 3\,\mathrm{kpc}$; $\chi^2/\mathrm{dof} = 7.5$.

with the dwarf companion DDO 44, which is undergoing tidal disruption with a stream extending on both sides of NGC 2403 across a range comparable to the full radial extent of the rotation curve data used here [1]. The outer rotation-curve region is therefore plausibly perturbed from axisymmetric equilibrium, and the spherically symmetric stationary configuration assumed in the present analysis would be expected to show residuals of precisely the kind observed. Second, the piecewise Heaviside transition between inner core and outer halo in equation (50) represents an idealisation of the smooth domain-wall profile derived in the framework's vacuum structure document [4]. A tanh-smoothed transition introduces an additional width parameter and can be expected to reduce residuals of the sort seen in NGC 2403 without altering the parameter class; we have not implemented this refinement in the present fit. Both considerations suggest that the NGC 2403 residual does not constitute evidence against the framework's profile class but rather against the specific idealisations under which it has been tested.

6.6 Summary of the Empirical Test

The framework's multi-branch profile, applied in its simplest piecewise form and using closed-form enclosed mass expressions, fits thirteen SPARC galaxies spanning the morphological range at reduced chi-squared values below eleven for twelve of the thirteen galaxies, with nine below two. The profile parameters vary continuously across the sample in a manner that correlates with galaxy morphology: halo-dominated configurations for massive spirals with flat outer plateaus, core-dominated configurations for dwarf irregulars with rising curves, hybrid configurations for intermediate systems. The dark-matter-deficient galaxies recover purely baryonic kinematics as the limiting case where coherence densities vanish. A single marginal case, NGC 2403, shows residuals at the few-percent level consistent with known

Galaxy	ρ_c ($M_\odot$/kpc^3)	R_1 (kpc)	ρ_0 ($M_\odot$/kpc^3)	r_0 (kpc)	χ^2/dof	Morphology
F583-1	10^6	8	3×10^7	2	0.43	LSB
NGC 0100	10^7	3	10^7	5	0.40	Scd spiral
NGC 7814	10^7	8	3×10^7	5	0.74	Edge-on early spiral
NGC 3109	10^7	2	10^7	5	0.75	Small spiral
NGC 0024	10^8	2	3×10^7	3	1.51	Sc spiral
DDO 168	10^7	3	10^7	2	1.58	Dwarf irregular
NGC 0055	3×10^6	8	10^7	2	1.59	Magellanic-type
IC 2574	10^6	3	3×10^6	10	1.60	Large dwarf irregular
NGC 2841	3×10^7	5	3×10^8	2	2.10	Bulge-dominated spiral
NGC 6503	3×10^7	2.5	3×10^7	3	3.22	Sc spiral
DDO 154	5×10^6	2.5	10^7	3	7.47	Dwarf irregular
NGC 3198	10^7	3	5×10^7	2.5	8.83	Sc spiral
NGC 2403	3×10^6	6	7×10^7	2	17.82	Sc spiral

Table 1: Best-fit parameters for the thirteen SPARC galaxies analysed in this work. The profile is defined in equation (50) and the enclosed mass in equation (51). All fits use $\Upsilon_{\star,\mathrm{disk}} = 0.5$ and $\Upsilon_{\star,\mathrm{bulge}} = 0.7$. Ordering is by increasing χ^2/dof.

tidal perturbation and the Heaviside idealisation of the core-to-halo transition.

Within the restricted scope of this test, the framework's density profile class is empirically consistent with observed galaxy rotation curves across the morphological range probed here. The test is a first confrontation rather than a definitive validation: the four fitted parameters per galaxy are not yet derived from the underlying Taiji–Skyrme couplings, the sample is not yet large enough to test population-level correlations such as the baryonic Tully–Fisher relation, and the idealisations of spherical symmetry and piecewise-constant branches await refinement. These directions are taken up in the following sections.

7 Tully–Fisher-Type Scaling under Coherence Hypotheses

Observed spiral galaxies exhibit a correlation between the asymptotic rotation velocity v_∞ and the total baryonic mass M_b, often summarised as a Tully–Fisher-type scaling

$$v_\infty^4 \propto M_\mathrm{b}. \tag{53}$$

Within the coherence-based framework, this relation is not automatic; it emerges, if at all, under additional hypotheses relating coherence sector parameters across families of galaxies.

Assume that at large radii the coherence-induced contribution dominates the rotation curve and provides an approximately constant velocity scale v_coh:

$$v_\infty^2 \simeq v_\mathrm{coh}^2 \simeq 4\pi G \rho_0 r_0^2, \tag{54}$$

with ρ_0 and r_0 parameters characterising the outer coherence profile (44). Then

$$v_\infty^4 \simeq 16\pi^2 G^2 \rho_0^2 r_0^4. \tag{55}$$

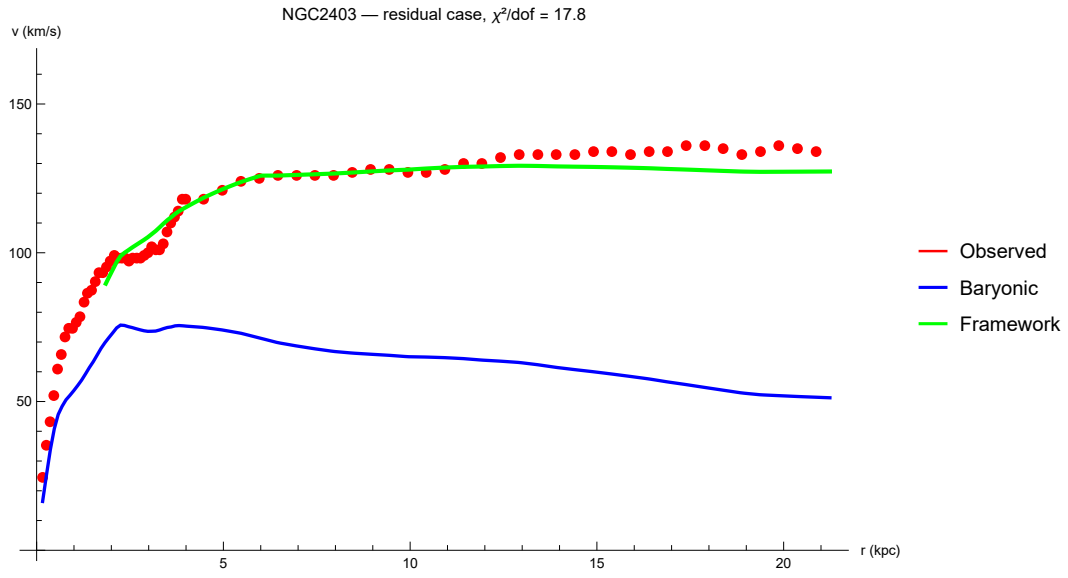

Figure 4: Rotation curve fit for NGC 2403. Best-fit parameters: $\rho_c = 3 \times 10^6$, $R_1 = 6\,\mathrm{kpc}$, $\rho_0 = 7 \times 10^7$, $r_0 = 2\,\mathrm{kpc}$; $\chi^2/\mathrm{dof} = 17.8$. The framework reproduces the gross morphology and a subtle inner inflection near $r = 3\,\mathrm{kpc}$ visible in the data, but systematically underpredicts the plateau amplitude by approximately 2–3%.

To relate this to M_b, one needs a structural relation of the form

$$\rho_0^2 r_0^4 \propto M_b. \tag{56}$$

Such a relation could arise if the coherence sector parameters (ρ_0, r_0) are not independent of the baryonic component, but are instead tied to it through:

- a common dependence on microscopic couplings $(f, e, v, C_\star, \alpha_C)$,
- and a selection mechanism in galaxy formation that correlates the characteristic coherence scale with the baryonic mass.

For example, if one postulates that

$$\rho_0 \sim \rho_\star, \qquad r_0^2 \sim \frac{M_b}{\rho_\star}, \tag{57}$$

for some quasi-universal density scale $\rho_\star$ set by coherence physics, then

$$\rho_0^2 r_0^4 \sim \rho_\star^2 \left(\frac{M_b}{\rho_\star}\right)^2 \propto M_b^2, \tag{58}$$

which would lead to $v_\infty^4 \propto M_b^2$ rather than the desired linear scaling. To obtain $v_\infty^4 \propto M_b$, one would instead require

$$\rho_0^2 r_0^4 \propto M_b, \tag{59}$$

for example through

$$\rho_0 \sim \rho_\star, \qquad r_0^2 \sim \frac{M_{\rm b}}{\rho_\star^2}, \tag{60}$$

or other combinations that correlate the coherence scale r_0 more strongly with the baryonic mass.

The main point is that, within the present coherence-based phenomenology:

- a flat outer rotation curve can arise naturally from a coherence-induced $1/r^2$ density tail,
- but a Tully–Fisher-type scaling $v_\infty^4 \propto M_{\rm b}$ is not guaranteed; it requires additional structural relations between coherence profile parameters and $M_{\rm b}$.

Determining whether such relations can be derived from the underlying Taiji–Skyrme dynamics and typical galaxy formation scenarios is a separate problem that lies beyond the scope of this phenomenological overview.

MOND-like target curves and residuals

Modified Newtonian Dynamics (MOND) provides a phenomenological benchmark for galactic rotation curves via a characteristic acceleration scale a_0. In the deep-MOND regime the asymptotic circular velocity for a purely baryonic mass $M_{\rm b}$ satisfies

$$v_{\rm MOND}^4 = G\, a_0\, M_{\rm b}, \tag{61}$$

so that

$$v_{\rm MOND} = (G a_0 M_{\rm b})^{1/4} \tag{62}$$

sets a target flat-curve scale.

In the coherence-based framework developed here the outer rotation curve is instead obtained from the total circular velocity (17), with the flat part dominantly controlled by the halo and environmental contributions,

$$v_{\rm tot}^2(r) \simeq \sum_{b\in\mathcal{B}_{\rm halo}} v_{{\rm h},b}^2(r) + v_{\rm env}^2(r), \qquad r_{\rm flat} \lesssim r \lesssim r_{\rm max}. \tag{63}$$

To quantify how closely a given parameter choice in the coherence sector matches a MOND-like target, we may define a dimensionless residual

$$\Delta_{\rm MOND}(r) = \frac{v_{\rm tot}(r) - v_{\rm MOND}}{v_{\rm MOND}}, \tag{64}$$

and study its magnitude over the approximately flat region. The phenomeno- logical goal is to identify parameter ranges for which

$$\sup_{r_{\rm flat}\le r\le r_{\rm max}} |\Delta_{\rm MOND}(r)| \lesssim 0.1, \tag{65}$$

i.e. the total coherence-based rotation curve tracks a MOND-like flat velocity within $\mathcal{O}(10\%)$. Demonstrating whether such parameter choices exist, and how they depend on the underlying Taiji–Skyrme couplings, requires dedicated numerical exploration and lies beyond the scope of the present analytic overview.

8 Phenomenological Regimes, Constraints, and Limitations

The coherence-based galaxy models discussed above are intended as structurally consistent, but deliberately simplified, phenomenological constructions. Several limitations and open issues must be kept explicit:

- **Spherical symmetry.**
  Real galaxies possess discs, bulges, and non-spherical halo components. The present analysis uses spherical symmetry to extract qualitative behaviour and should be regarded as a first approximation. A more realistic treatment would require at least axisymmetric configurations and disc-like baryonic distributions.

- **Effective density profiles vs microscopic fields.**
  The profiles $\rho_{\mathrm{coh}}(r)$ used here are phenomenological summaries of much more detailed coherence and Skyrme configurations. A full derivation would start from the coupled field equations for U and ψ in a galactic background and solve for $\psi(r)$, $U(r)$ (or more general spatial dependence), and hence $T_{00}[U, \psi](r)$.

- **Parameter degeneracies.**
  Many combinations of (ρ_0, r_0) and baryonic distributions can produce similar rotation curves. Without additional constraints from, for example, lensing or vertical dynamics, the coherence parameters remain underdetermined in these simple models.

- **Tully–Fisher scaling.**
  The emergence of a Tully–Fisher-type relation depends on nontrivial correlations between coherence and baryonic parameters across galaxy families. These correlations are not derived here; they are only outlined as potential structural conditions.

- **Time dependence and formation history.**
  Galaxies form and evolve through complex processes, including mergers, feedback, and environmental effects. Static, spherically symmetric models capture only the end-state kinematics, not the dynamical path by which coherence branches are populated and domain-wall networks are arranged.

- **Cosmological consistency.**
  Any coherence-based explanation of galaxy rotation curves must ultimately be compatible with cosmological constraints such as the cosmic microwave background and large-scale structure. The necessary cosmological analysis is deferred to separate work focused on coherence cosmology.

Despite these limitations, the present phenomenological framework provides a consistent way to:

1. translate coherence vacuum structure and domain walls into effective halo-like density profiles,

2. compute the resulting rotation curves within standard gravity,

3. and identify qualitative conditions for flat outer velocities and possible mass–velocity correlations.

It thereby serves as a bridge between the field-theoretic coherence sector and observable galactic dynamics.

9 Summary and Outlook

We have constructed a coherence-based phenomenological framework for galaxy rotation curves within the Taiji–Skyrme theory. Starting from the normalised coherence field ψ, its multi-vacuum structure, and domain walls, and using the unified parameter mapping and general-relativistic coupling, we built spherically symmetric models in which:

- the effective mass density is decomposed into baryonic and coherence-structured components, with the electromagnetic contribution present in the full Taiji–Skyrme–Maxwell theory but negligible in the galactic regimes considered here (so that $T_{00}^{(\mathrm{EM})} \simeq 0$ at the phenomenological level),
- coherence branches and their interfaces give rise to core and halo-like density contributions,
- and the resulting rotation curves are computed in the Newtonian limit as functions of the effective density profiles.

We showed that:

- inner regions with approximately constant coherence-induced densities lead to rising contributions to the rotation curve,
- outer regions with effective coherence density falling approximately as $1/r^2$ can produce flat rotation-curve plateaus,
- and Tully–Fisher-type scalings require additional structural correlations between coherence-profile parameters and the baryonic mass.

Throughout, gravity is treated purely within general relativity, with the total stress–energy tensor $T_{\mu\nu}^{\mathrm{tot}}$ as the unique source; no independent coherence-force law is introduced. The Maxwell sector enters this tensor in the standard way, but for the spherically symmetric galaxy models studied here we work in an electromagnetically silent regime consistent with $\rho_{\mathrm{EM}} \ll \rho_b, \rho_{\mathrm{coh}}$.

The next steps in making this framework quantitatively predictive are:

1. solving the coupled field equations for U and ψ in simplified galactic configurations to derive $\rho_{\mathrm{coh}}(r)$ from first principles,

2. extending the models to axisymmetric geometries with realistic baryonic discs,

3. and confronting the resulting rotation curves with observational data, including the scatter and systematics of the Tully–Fisher relation.

These tasks lie beyond the scope of the present phenomenological overview, but the structure developed here provides a consistent starting point for such investigations and integrates coherently with the broader Taiji–Skyrme framework.

References

[1] Jeffrey L. Carlin, Christopher T. Garling, Annika H. G. Peter, Denija Crnojević, Duncan A. Forbes, Jonathan R. Hargis, Burçin Mutlu-Pakdil, Ragadeepika Pucha, Aaron J. Romanowsky, David J. Sand, Kristine Spekkens, Jay Strader, and Beth Willman. Tidal Destruction in a Low-mass Galaxy Environment: The Discovery of Tidal Tails around DDO 44. *The Astrophysical Journal*, 886(2):109, 2019. doi: 10.3847/1538-4357/ab4c32.

[2] Michael A. Keim, Pieter van Dokkum, Shany Danieli, et al. A Third Galaxy Missing Dark Matter along a Trail of Galaxies in the NGC 1052 Field. *arXiv preprint*, 2026. arXiv:2603.15860.

[3] Federico Lelli, Stacy S. McGaugh, and James M. Schombert. SPARC: Mass Models for 175 Disk Galaxies with Spitzer Photometry and Accurate Rotation Curves. *The Astronomical Journal*, 152(6):157, 2016. doi: 10.3847/0004-6256/152/6/157.

[4] Eduardo R. Santibañez Mugica. Coherence Vacuum Structure and Domain Walls in the Taiji–Skyrme Framework. Internal document, 2026.

[5] Eduardo R. Santibañez Mugica. Dark Matter Separability and the Bullet Dwarf Collision Scenario. Internal report, 2026.

[6] James Schombert, Stacy McGaugh, and Federico Lelli. The mass-to-light ratios and the star formation histories of disc galaxies. *Monthly Notices of the Royal Astronomical Society*, 483(2):1496–1512, 2019. doi: 10.1093/mnras/sty3223.

[7] Pieter van Dokkum et al. A galaxy lacking dark matter. *Nature*, 555:629–632, 2018.

[8] Pieter van Dokkum et al. A Second Galaxy Missing Dark Matter in the NGC 1052 Group. *The Astrophysical Journal Letters*, 874(1):L5, 2019.